

Article

Investigation of Major Flavonoids from *Artemisia argyi* as a Potential COVID-19 Drug: Molecular Docking and DFT Calculations

Yang Lu ^{1,*}, Bin Zhang ^{2,*} , Ning Wang ¹, Mengshan Li ³ and Ning Xi ^{1,*}¹ Institute of Drug Discovery Technology, Ningbo University, Ningbo 315211, China; wangning@nbu.edu.cn² Li Dak Sum Yip Yio Chin Kenneth Li Marine Biopharmaceutical Research Center, Department of Marine Pharmacy, College of Food and Pharmaceutical Sciences, Ningbo University, Ningbo 315800, China³ College of Geriatric Education, Ningbo Open University, Ningbo 315211, China; lims@nbou.cn

* Correspondence: luyang@nbu.edu.cn (Y.L.); zhangbin1@nbu.edu.cn (B.Z.); xining@nbu.edu.cn (N.X.)

Abstract: Flavonoids from natural products are well-identified as potential antiviral agents in the treatment of SARS-CoV-2 (COVID-19) infection and related diseases. However, some major species of flavonoids from Chinese traditional folk medicine, such as of *Artemisia argyi* (*A. argyi*), have not been evaluated yet. Here, we choose five major flavonoids obtained from *A. argyi*, namely, Jaceosidin (1), Eupatilin (2), Apigenin (3), Eupafolin (4), and 5,6-Dihydroxy-7,3',4'-trimethoxyflavone (5), compared to the well-studied Baicalein (6), as potential inhibitors analogs for COVID-19 by computational modeling strategies. The frontier molecular orbitals (FMOs), chemical reactivity descriptors, and electrostatic surface potential (ESP) were performed by density functional theory (DFT) calculations. Additionally, these flavonoids were docked on the main protease (PDB: 6LU7) of SARS-CoV-2 to evaluate the binding affinities. Computational analysis predicted that all of these compounds show a high affinity and might serve as potential inhibitors to SARS-CoV-2, among which compound (5) exhibits the least binding energy (−155.226 kcal/mol). The high binding affinity could be enhanced by increasing the electron repulsion due to the valence shell electron pair repulsion model (VSEPR). Consequently, the major flavonoids in *Artemisia argyi* have a significant ability to reduce the deterioration of COVID-19 in the terms of DFT calculations and molecular docking.

Keywords: *Artemisia argyi*; flavonoids; COVID-19; DFT calculations; molecular docking



Citation: Lu, Y.; Zhang, B.; Wang, N.; Li, M.; Xi, N. Investigation of Major Flavonoids from *Artemisia argyi* as a Potential COVID-19 Drug: Molecular Docking and DFT Calculations. *Crystals* **2022**, *12*, 990. <https://doi.org/10.3390/cryst12070990>

Academic Editor: Sergio Brutti

Received: 6 June 2022

Accepted: 12 July 2022

Published: 16 July 2022

Publisher's Note: MDPI stays neutral with regard to jurisdictional claims in published maps and institutional affiliations.



Copyright: © 2022 by the authors. Licensee MDPI, Basel, Switzerland. This article is an open access article distributed under the terms and conditions of the Creative Commons Attribution (CC BY) license (<https://creativecommons.org/licenses/by/4.0/>).

1. Introduction

Novel coronavirus (COVID-19), caused by severe acute respiratory syndrome coronavirus 2 (SARS-CoV-2), with spread by saliva or secretions from the nose when infected people sneeze or cough [1–3], and has spread rapidly to all countries, with more than 529 million infections and 6.3 million deaths worldwide to date (13 July 2022). Human coronavirus was first discovered in the mid-1960s and is well-known as a general pathology in a large extent of common respiratory tract infections [4]. Coronaviruses belong to a family of the single-stranded positive-sense RNA, in which they were divided into α , β , γ , and δ genera. The α and β genera of coronaviruses normally infect mammals such as humans, while γ and δ genera generally infect birds [5]. The COVID-19, first reported in Wuhan, belongs to the β genera and is identified as a typical crown-shaped structure of coronavirus being 60–140 nm in diameter. Additionally, the incubation period of COVID-19 ranges from 2 to 14 days [6,7]. Moreover, the SARS-CoV-2 pandemic has proceeded in multiple waves and is driven by the emergence of successive variants such as Alpha, in late 2020, and was succeeded by Delta in the early portion of 2021. Until now, Omicron displaced Delta as the most widely transmitted strain since late 2021, which results in millions of infected persons per day [8]. In general, eliminating the source of infections by wearing a mask and disinfecting the virus is the main way to control COVID-19's propagation. Additionally,

several vaccines and approved drugs have been proved to be efficient to protect and treat the disease [9].

However, the number of infections is still growing exponentially in many districts and the post-COVID symptoms remain poorly defined [10]. It has been reported that natural products could offer effective antiviral activity against SARS-CoV-2 [11–13]. For instance, Lianhuaqingwen capsules, processed from a variety of Chinese herbal medicines, have been shown to have clinical improvement and curative ratios enhanced by 19.8% and 12.7%, respectively, compared to the control group [14]. Moreover, the anti-coronavirus effects of natural products have been confirmed in vitro, and in silico studies assume that the antiviral effect may be caused by blocking the coronavirus main protease [12]. So, investigating the potential use of protease inhibitors is meaningful to rationalize the treatment against infections of SARS-CoV-2. Nevertheless, one of the famous Chinese traditional herbs, *Artemisia argyi* (*A. argyi*), has not been evaluated as yet. Ancient Chinese commonly pick the leaves of *A. argyi* to control rheumatism, abdominal pain, dysmenorrhea, and inflammation. Additionally, *A. argyi* contains a large number of flavonoids that show various biological activities such as antiviral, antioxidant, and anti-inflammatory activities [15–17]. Though many studies revealed that some flavonoids could be a potential prophylaxis against SARS-CoV-2 [18–20], the major species in *A. argyi*, Jaceosidin (1), Eupatilin (2), Apigenin (3), Eupafolin (4), and 5,6-Dihydroxy-7,3',4'-trimethoxyflavone (5), remained to be explored.

With those in mind, computational aspects offer novel reasonable hypotheses for potential drugs against COVID-19, and a virtual screening technique was well developed to estimate the active binding site on the target protease for many natural compounds through molecular docking [21–28]. Our research group is interested in the studies of the structure–activity relationships (SARs) of natural compound derivatives by organic synthesis, biological evaluation, and molecular docking studies to provide theoretical guidance for further drug development [29,30]. Hence, our present work selects five major flavonoids that are special or major located in *A. argyi* to perform the in silico study of their antiviral activity against SARS-CoV-2. Moreover, one well-studied flavonoid Baicalein (6) was selected as the reference, which has proved to be a potential drug against SARS-CoV-2 [31,32].

2. Materials and Methods

2.1. Density Functional Theory (DFT) Calculations

Gaussian 16 program package was used to perform the geometrical and electronic properties of target flavonoids 1–6. The calculation mode of B3LYP (Becke three parameters hybrid functional with Lee–Yang–Perdew correlation functionals) and the 6–311G(d) atomic basis set was adopted. Additionally, the molecular orbitals and electrostatic surface potential (ESP) were visualized using Gaussview 6.0.

2.2. Molecular Docking Protocol

The 2019-nCoV protease crystal structure (PDB: 6LU7) was downloaded from the RCSB protein data bank. The CDOCKER procedure of Discovery Studio 2020 software has been used to explore the binding modes of compounds 1–6 with 2019-nCoV protease. The target protein was prepared for docking by the automatic “prepare protein” procedure, including removing water molecules, adding hydrogen atoms, and protonating amino acids residing at the specified pH of 7.4. The 3D structures of compounds 1–6 were built and prepared by the “prepare ligands” procedure. The coordinate used for the binding site of 2019-nCoV protease was x: −10.742772; y: 12.459444; z: 68.917978 with a radius 17.82 Å.

2.3. Molecular Dynamics (MD) Simulation

The MD simulation was performed by Discovery Studio 2020 software using the biases of CDOCKER data. The pre-reaction state was treated with the CHARM36 force field. An explicit solvation process was applied to the system under periodic boundary conditions. The system was performed by a 200 ns MD simulation at 300 K. The post-MD

calculation was from the discovery studio 2020 directly, and the captured pictures were from the MD-simulation video at different times.

3. Results and Discussions

3.1. DFT Calculations Studies

Compounds 1–6 were optimized by the DFT calculations, which were performed in the gas phase with the Gaussian 16 (Pittsburgh, PA, USA) program package using B3LYP (Becke Three Parameters Hybrid Functional with Lee–Yang–Perdew correlation functions) with the 6-311G(d) atomic basis set. Additionally, the thermal parameters, dipole moment, and the polarizability of compounds 1–6 are shown in Figure 1.

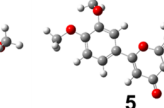
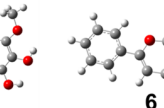
Structures						
Total Dipole Moment	5.02 Debye	5.51 Debye	4.24 Debye	5.51 Debye	6.40 Debye	6.37 Debye
Polarizability α	228.25 a.u.	243.62 a.u.	192.16 a.u.	214.99 a.u.	243.42 a.u.	188.57 a.u.

Figure 1. Optimized geometrical structures, dipole moment, and the polarizability of compounds 1–6.

The DFT-calculated data revealed that the dipole moment of these six flavonoids was in the order of $3 < 1 < 2 < 4 < 6 < 5$. Additionally, the highest value of dipole moment for compound 5 was 6.40 Debye among the studied flavonoids, and a high dipole moment leads to a high polarizability, according to the ratio of dipole moment to electric field intensity [33]. The polarizability is defined as the ease of electron cloud distortion affected by an approaching charge and is very valuable in the correlation of allosteric effects in drug–protease interactions. It is worth to know that compound 6 also has a high dipole moment but low polarizability. The high dipole moment and polarizability of compound 5 could benefit the binding pose within a specific target protein and enhance binding affinity, which will be discussed in the following molecular docking studies.

3.1.1. Frontier Molecular Orbitals

Frontier molecular orbitals (FMOs) theory is always used to explain the organic reaction mechanisms, which is also meaningful in the analysis of the interaction between drugs and their receptors. FMOs contain the highest occupied molecular orbital (HOMO) and the lowest unoccupied molecular orbital (LUMO). The electrons in HOMO are weakly attached so they can be donated to the LUMO-type molecular orbitals as an electron donor, while the empty LUMO always acts as an electron acceptor to accept electrons. The distribution and the energy gap (E_g) of HOMO and LUMO for investigated flavonoids are shown in Figure 2.

Recently, studying FMOs theory has become increasingly important to investigate the structure–activity relationships of small structural drugs [34–36]. As flavonoids 1–6 are all highly conjugated systems, the HOMOs and LUMOs distributions are all mainly located in the aromatic systems with poor separations except compound 5 and compound 6. Additionally, the energies of HOMOs and LUMOs are also within a narrowed range, of which the HOMO was from -6.08 eV to -5.71 eV and the LUMO was from -1.81 eV to -1.51 eV. Nevertheless, compound 5 stated the most lying HOMO energy than the other flavonoids, which means it could be a better electron donor in drug–receptor systems by increasing the binding affinity. Consequently, compound 5 owns the narrowest energy

gap (4.20 eV) among the five flavonoids in *A. argyi*. The HOMO distribution of compound 5 is mainly located in the chromone ring, while the LUMO distribution is all dispersed on the full molecular. Although the energy gap (4.10 eV) of compound 6 is smaller than compound 5, its HOMO energy level is also much shallower, indicating it as a worse electron donor. The high lying HOMO, less E_g , and good HOMO separation indicate that charge transfer is possible with a greater binding affinity than would be expected.

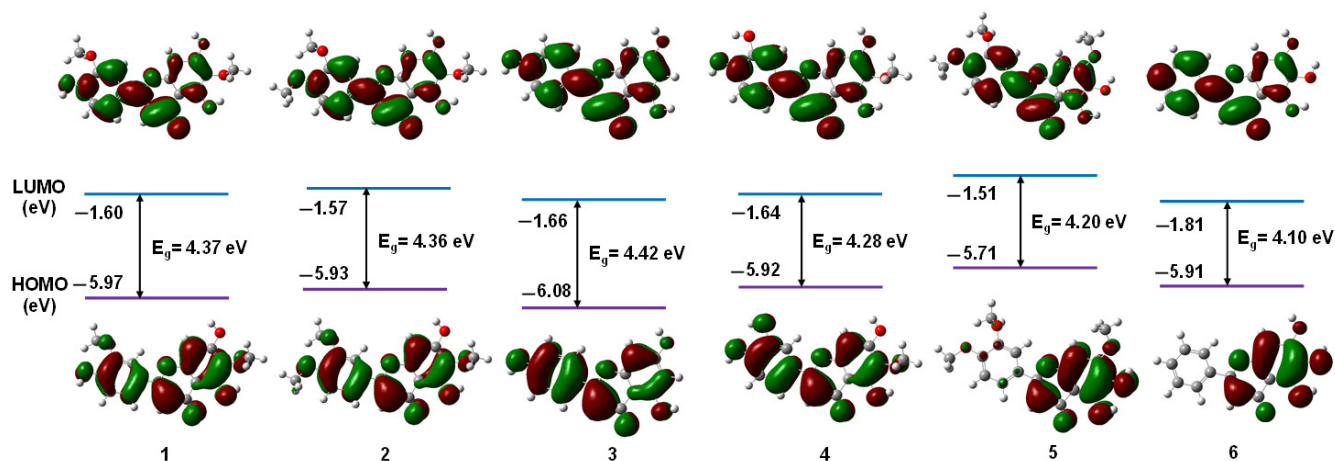


Figure 2. The energy gap and distribution of HOMO and LUMO of compounds 1–6.

3.1.2. Chemical Reactivity Descriptors

Additionally, other chemical reactivity descriptors also have been estimated, such as electronegativity (χ), global hardness (η), softness (δ), electrophilicity (ω), ionization energy (IE), and electron affinity (EA), as listed in Table 1. IE was calculated by the energy difference between +1 charged molecules and uncharged molecules while EA was calculated by the energy difference between -1 charged molecules and uncharged molecules. Additionally, the rest of the descriptors are calculated according to the Equations (1)–(4):

$$\chi = -\frac{1}{2}(E_{HOMO} + E_{LUMO}) \quad (1)$$

$$\eta = -\frac{1}{2}(E_{HOMO} - E_{LUMO}) \quad (2)$$

$$\delta = \frac{1}{\eta} \quad (3)$$

$$\omega = \frac{\chi^2}{2\eta} \quad (4)$$

The χ value is the tendency of the molecule to attract electrons, namely, the large values of (χ) are a Lewis acid while small values are an indication of a Lewis base. The global hardness (η) states the degree of resistance to deformation of the electron cloud of molecules; on the contrary, the global softness (δ) is defined as the inverse of the ability to accept electrons of molecules. According to the definition, soft molecules are always with narrow bandgaps and are more reactive than hard because electron transfer could happen more easily. The electrophilicity (ω) is calculated from chemical hardness and electronegativity as an indicator of the energy difference between the donor and acceptor [37]. Additionally, ionization energy (IE) and electron affinity (EA) represent the electron-donating and electron-accepting abilities of molecules, respectively. Accordingly, the relatively small χ (3.61 eV), η (2.10 eV), ω (3.10 eV), A (0.35 eV), and large δ (0.48 eV) of compound 5 indicate that it is more reactivity to affect by target protease, which also has been discussed in the following molecular docking part.

Table 1. Calculated electronegativity (χ), global hardness (η), softness (δ), global electrophilicity index (ω), the ionization potential (I), and the electron affinity (A) (eV) of investigated flavonoids 1–6.

Flavonoids	1	2	3	4	5	6
E_{HOMO}	−5.97	−5.93	−6.08	−5.92	−5.71	−5.91
E_{LUMO}	−1.60	−1.57	−1.66	−1.64	−1.51	−1.81
ΔE	4.37	4.36	4.42	4.28	4.20	4.10
χ	3.79	3.75	3.87	3.78	3.61	3.86
η	2.19	2.18	2.21	2.14	2.10	2.05
δ	0.46	0.46	0.45	0.47	0.48	0.49
ω	3.28	3.23	3.39	3.34	3.10	3.63
I	7.19	7.12	7.43	7.14	7.05	7.40
A	0.43	0.42	0.36	0.43	0.35	0.52

3.1.3. Electrostatic Surface Potential (ESP)

Electrostatic surface potential (ESP) reflects the molecular nucleophilicity of which red represents nucleophilic regions while blue represents electrophilic regions. It can be calculated by considering the molecular orbitals and identifying how compounds with different structures might line up to interact with corresponding electron-rich and electron-poor areas in binding sites such as protease receptors [38].

The ESP of the studied flavonoids (1–6) was calculated by the DFT method under the same base sets by Gaussian 16 software as depicted in Figure 3. The large absolute value of the maximum negative region (red part) represents the ability of nucleophilicity (the numbers represent the maximum negative region), which is in the order of $3 < 6 < 1 < 2 < 4 < 5$. Surprisingly, compound 5 owns the maximum value among these flavonoids (-8.80×10^{-2} a.u.). This result is totally in line with the FMO studies that we discussed above, indicating that compound 5 has a better reactivity with receptors. Furthermore, we could observe that the most nucleophilicity parts for all studied flavonoids are around the ketone and nearby hydroxy group in chromone cores. As is well known, the stability of molecules follows the valence-shell electron pair repulsion model (VSEPR). However, the adjacent oxygen atoms with negatively charged electron lone pairs are locked in the rigid structure, namely, they are not stable and easily give electrons to release the repulsion. The repulsions in compound 3, compound 5, and compound 6 are the most rigid ones with no torsion angle at all (0.0°). However, electron-donating groups in compound 3 and compound 6 are less than the ones in compound 5. Additionally, the electron-donating ability of the hydroxy group is also weaker than the methoxy group, which resulted in weaker nucleophilicity. The ESP studies could offer a principally responsible mechanism for their binding affinity with active receptors.

3.2. Molecular Docking Studies

Molecular docking studies of compounds 1–6 with 2019-nCoV protease (PDB: 6LU7) showed that these five compounds had similar binding modes. The binding energy of compounds 1–6 ranged from -122.010 to -155.226 kcal/mol as presented in Table 2. From the docking mode of compound 1 with 2019-nCoV protease (Figure 4), it can be seen that the carbonyl group and the 5-hydroxyl group on its flavonoid backbone formed three traditional hydrogen bonds with residues HIS163 and LEU141, respectively. However, there was an unfavorable donor–donor interaction between the 5-hydroxyl group and the amino acid SER144. In addition, the methoxy group on the 2-phenyl group (B ring) formed multiple carbon–hydrogen bonds with multiple amino acid residues such as GLU166 and LEU167. Moreover, compound 1 had van der Waals interactions with residues GLN189 and HIS172. Unfortunately, the other two hydroxyl groups on the A ring and the B ring failed to form hydrogen bonds with the residues. The binding energy of compound 1 to the target protein was -142.277 kcal/mol.

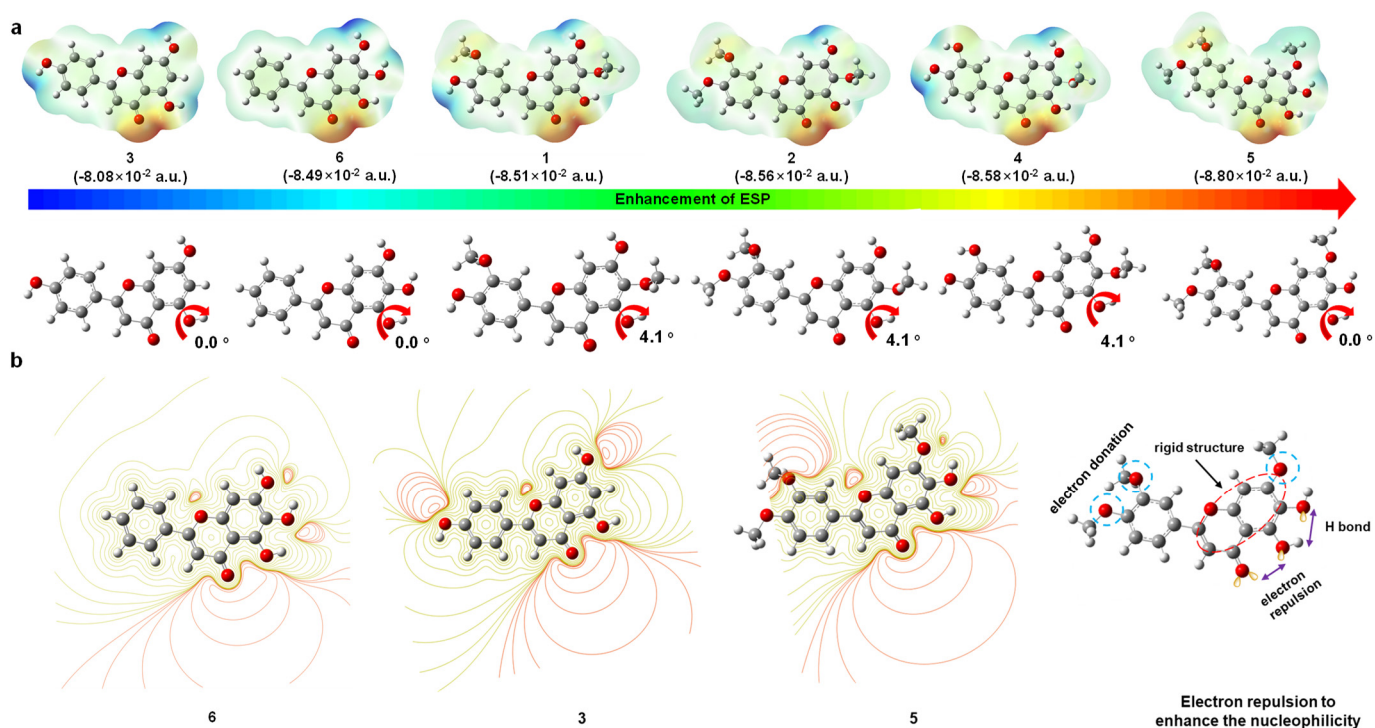
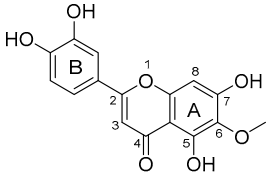
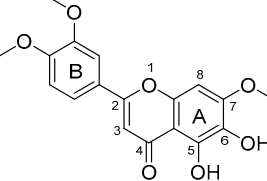
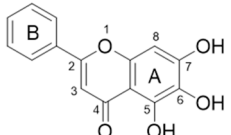


Figure 3. (a). The electrostatic surface potentials of compounds 1–6 and dihedral angles of hydroxy group in chromone. (b). The illustration of electron repulsion.

Table 2. Data analysis of the flexible docking of compounds 1–6 in the active site of the 2019-nCoV protease receptor.

Compounds	Structures	Binding Energy (kcal/mol)	Amino Acids Residue of 2019-nCoV Protease
1		−142.277	LEU141, HIS163, GLU166 LEU167, HIS172, GLN189
2		−144.323	LEU27, LEU141, CYS145, HIS163, GLU166, LEU167, PRO168, GLN189
3		−122.010	LEU141, ASN142, CYS145, HIS163, GLU166, HIS172, GLN189

Table 2. Cont.

Compounds	Structures	Binding Energy (kcal/mol)	Amino Acids Residue of 2019-nCoV Protease
4		−151.706	HIS41, MET49, GLU166, CYC44, TYR54, ASN142, HIS164, GLN189
5		−155.226	HIS41, MET49, PRO52, TYR54, PHE140, LEU141, ASN142, SER144, HIS163, HIS164, MET165, GLU166, HIS172, ASP187, ARG188, GLN189, THR190, GLN192
6		−130.763	HIS41, SER144, GLY143, CYS145, GLU166

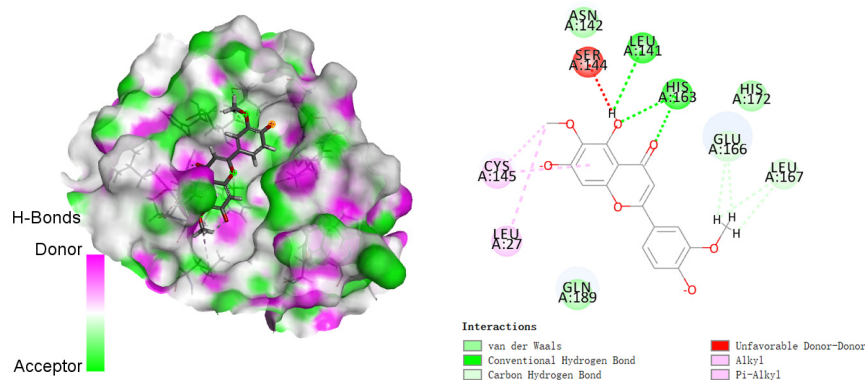


Figure 4. The binding mode of compound 1 (3D view and 2D view) with 2019-nCoV protease. The carbon atoms of compound 1 and 2019-nCoV protease are represented as grey sticks, and oxygen atoms are shown in red. All the nonbonded interactions are shown in dotted lines with different colors according to their different interaction properties.

The docking results of compounds 2–4 with the target protein were similar to that of compound 1, except that another traditional hydrogen bond was formed between the oxygen atom of the 6-methoxy group and the residue CYS145, as shown in Figure 5. It should be noted that the methyl group on the 6-methoxy group simultaneously formed two alkyl interactions with amino acid residues LEU27 and CYS145. From the structure of compound 2, there were two methoxy substitutions on the 2-phenyl group (B ring), one of which formed two carbon-hydrogen bonds with residues GLU166 and LEU167, and the other formed an alkyl interaction with PRO168. In addition, the Pi-Alkyl interaction between the A ring and CYS145 was generated, and there was also a van der Waals interaction between compound 2 and residue GLN189. The binding energy of compound 2 to the target protein was −144.323 kcal/mol. The main difference in the docking results of compound 3 is that one hydroxyl group on its 2-phenyl group (B ring) formed a traditional hydrogen bond with the residue GLU166, which also indicated the importance of hydroxyl substitution in the flavonoid backbone [39]. The binding energy of compound 3 to the target protein was −122.010 kcal/mol. For compound 4, the 5-hydroxyl group on the

A ring formed a traditional hydrogen bond with the residue HIS41, and the 6-methoxy group formed an alkyl group with HIS41 and MET49, respectively. In addition, the two hydroxyl groups on the 2-phenyl (B ring) formed one traditional hydrogen bond with GLU166, respectively. Moreover, compound 4 exhibited van der Waals forces with multiple amino acid residues such as CYC44, TYR54, ASN142, HIS164, and GLN189. The binding energy of compound 4 to the target protein was -151.706 kcal/mol.

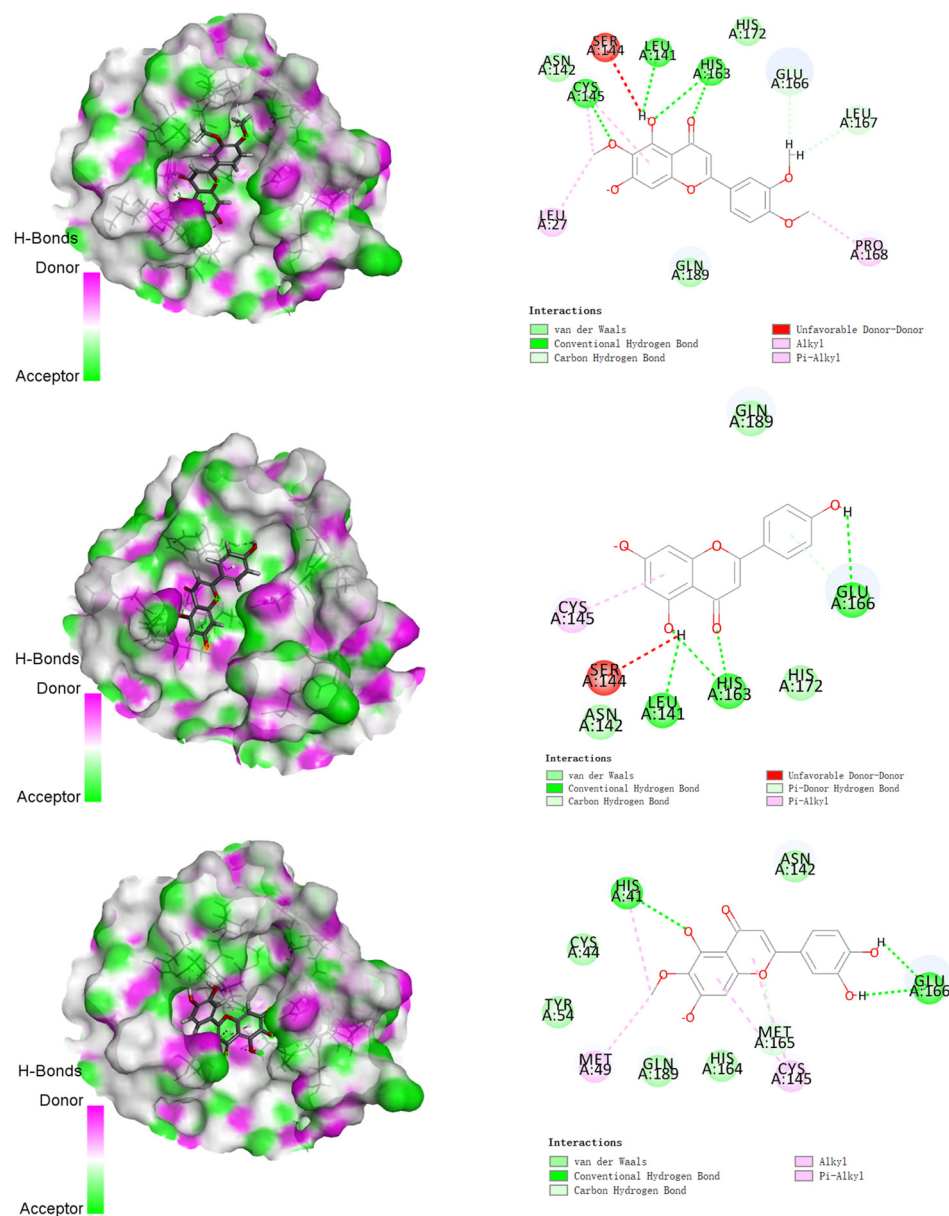


Figure 5. The binding mode of compound 2–4 (3D view and 2D view) with 2019-nCoV protease. The carbon atoms of compound 5 and 2019-nCoV protease were represented as grey sticks, and oxygen atoms were shown in red. All the nonbonded interactions are shown in dotted lines with different colors according to their different interaction properties.

Compared with compounds 1–4, compound 5 could better act in the pocket of 2019-nCoV protease (Figure 6). First, the 5-hydroxyl and 6-hydroxyl groups on the A ring formed three traditional hydrogen bonds with residues PHE140, HIS163, and GLU166, respectively, and the two hydroxyl groups on the B ring formed two carbon–hydrogen bonds with residues ASP187 and ARG188. Furthermore, the B-ring formed multiple alkyl or Pi-alkyl interactions with residues HIS41, MET49, and MET165. Moreover, compound 5

exhibited van der Waals forces with multiple amino acid residues such as PRO52, TYR54, LEU141, ASN142, SER144, HIS164, HIS172, GLN189, THR190, and GLN192. Among the five compounds, compound 5 had the lowest binding energy to the target protein, which was -155.226 kcal/mol. Additionally, the binding energy of Baicalein (6) to the target protein was -130.763 kcal/mol, which was only higher than compound 3. It well corresponded with the ESP studies and showed that all of the flavonoids in *A. argyi* could be potential anti-COVID-19 inhibitors.

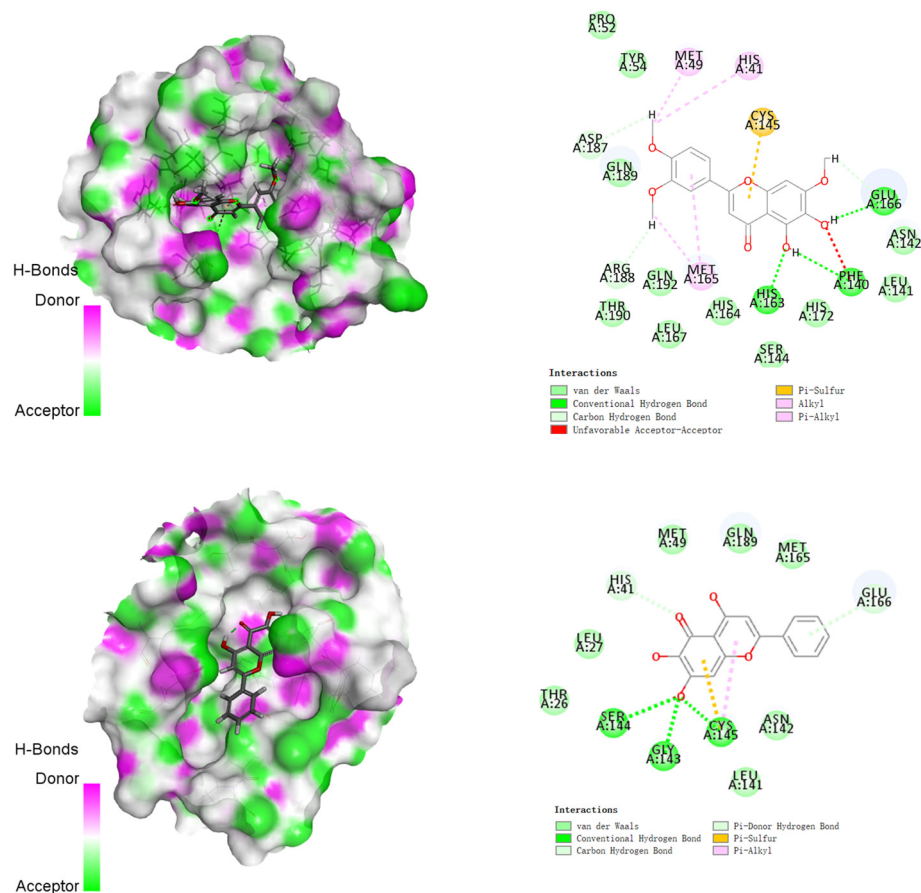


Figure 6. The binding mode of compound 5–6 (3D view and 2D view) with 2019-nCoV protease. The carbon atoms of compound 5 and 2019-nCoV protease are represented as grey sticks, and oxygen atoms are shown in red. All the nonbonded interactions are shown in dotted lines with different colors according to their different interaction properties.

Furthermore, in order to validate our docking studies, we performed the molecular dynamics (MD) simulation of compound 5, which was the most potential inhibitors in this study. Comfortingly, these results proved our discussion that the most electronegativity region (ketone and nearby hydroxy group in chromone cores) were the main part to bind with the protease, as shown in Figure 7a (we selected four pictures at different times from the MD video). Additionally, the heat map of the interaction binding sites showed more directly that the most reactive binding part is the two oxygen atoms as depicted in Figure 7b (the x axial represents the interaction mode, and the y axial represents the conformations of compound 5). Such results supported our analysis that the electron repulsion in the rigid structure would benefit the bioactivity.

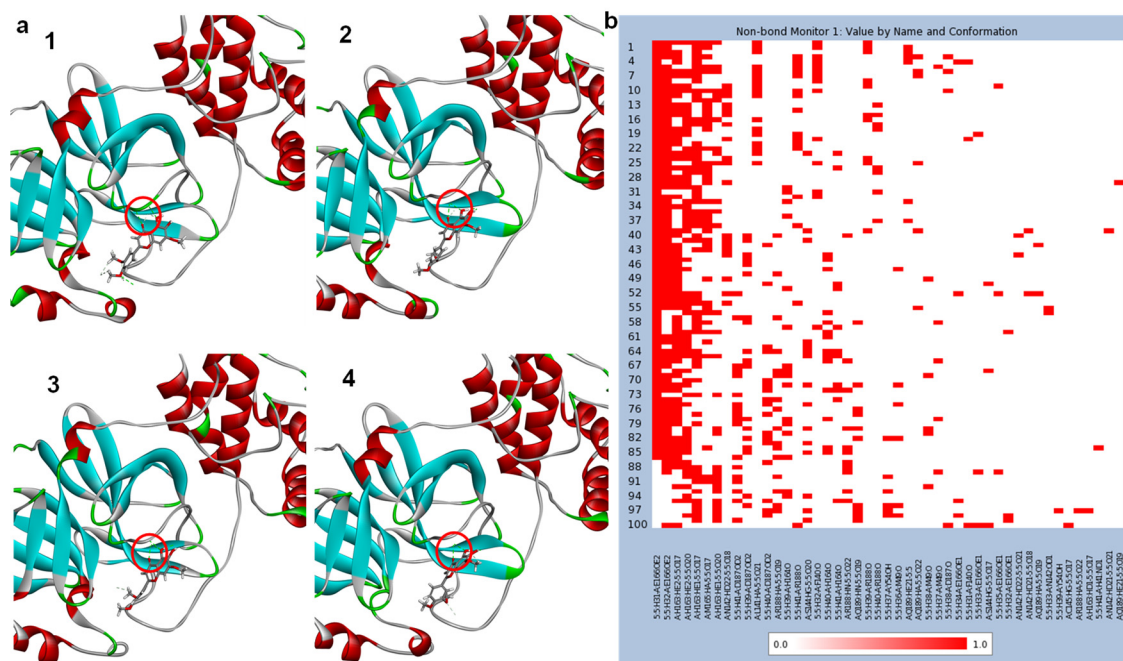


Figure 7. (a). Captured pictures from the MD-simulation video (red circle represents the main binding sites). (b). The heat map of binding sites between compound 5 with 2019-nCoV protease.

Finally, compared with the aforementioned data of DFT calculation and molecular docking studies, major flavonoids in *A. argyi* are possibly acted as protection and treatment against SARS-CoV-2. Hydrogen bonds and van der Waals interactions with the residues of target protease play a leading role in the binding affinity. Accordingly, the optimization of flavonoids with the more hydroxy groups and electron repulsion would benefit the activities by increasing the electron donor characters of these flavonoids and their derivatives. More specifically, a shallower HOMO and smaller χ , η , and ω could be efficient indicators for a better affinity of the drug–receptor interaction.

4. Conclusions

Five major flavonoids from *Artemisia argyi*, Jaceosidin (1), Eupatilin (2), Apigenin (3), Eupafolin (4), and 5,6-Dihydroxy-7,3',4'-trimethoxyflavone (5), compared with Baicalein (6), have been investigated as potential inhibitors for COVID-19 by DFT calculations and molecular docking studies. The results revealed that all of these flavonoids have good affinity with the target protease and 5,6-Dihydroxy-7,3',4'-trimethoxyflavone (5) shows the best affinity with the target protease receptor, with the lowest binding energy (−155.226 kcal/mol) compared with the other four flavonoids (3 > 1 > 2 > 4 > 5). Additionally, the DFT calculations revealed the structure–activity relationship (SAR) of the molecular docking results. Firstly, the most shallow HOMO of compound 5 (−5.71 eV) indicates the best electron donor it is, which means that compound 5 would show the most reactivity in the donor–receptor systems. Additionally, the rest of the chemical reactivity descriptors, such as a high softness ($\delta = 0.48$) and dipole moment ($\mu = 6.40$ Debye) of compound 5, could be the other factors that enhanced the binding affinity. Moreover, a small energy gap ($\Delta E = 4.20$ eV) between the HOMO and LUMO of compound 5 means that the electrons are flexible to transfer to increase the bioactivity. Furthermore, the ESP studies demonstrate that the strongest nucleophilicity region in the molecules is located in the rigid electron repulsion area of the chromone core according to the VSEPR theory, which is also correlated with docking studies essentially. Accordingly, the results discussed above indicate that compound 5 owns the most promising potential as an anti-COVID-19 inhibitor. More importantly, the DFT studies reveal that the improvement of the electron repulsion in the rigid structures

(i.e., ketone and hydroxy groups in chromone) would benefit the reactivity by releasing the repulsion; such results also would provide an efficient strategy for drug design.

Author Contributions: Conceptualization, Y.L. and N.W.; Funding acquisition, N.X.; Methodology, Y.L., B.Z. and N.W.; Project administration, N.X.; Supervision, Y.L., N.W. and N.X.; Visualization, B.Z.; Writing—original draft, B.Z. and M.L. All authors have read and agreed to the published version of the manuscript.

Funding: This research was funded by the Scientific Research Grant of Ningbo University (215-432000282), the Ningbo Top Talent Project (215-432094250), and the Natural Science Foundation of Ningbo City (2021J104).

Institutional Review Board Statement: Not applicable.

Informed Consent Statement: Not applicable.

Data Availability Statement: Not applicable.

Conflicts of Interest: The authors declare no conflict of interest.

References

1. Tao, K.; Tzou, P.L.; Nouhin, J.; Gupta, R.K.; de Oliveira, T.; Kosakovsky, P.S.L.; Fera, D.; Shafer, R.W. The biological and clinical significance of emerging SARS-CoV-2 variants. *Nat. Rev. Genet.* **2021**, *22*, 757–773. [[CrossRef](#)] [[PubMed](#)]
2. Diamanti, A.P.; Rosado, M.M.; Pioli, C.; Sesti, G.; Lagana, B. Cytokine Release Syndrome in COVID-19 Patients, A New Scenario for an Old Concern: The Fragile Balance between Infections and Autoimmunity. *Int. J. Mol. Sci.* **2020**, *21*, 3330. [[CrossRef](#)] [[PubMed](#)]
3. Song, W.-J.; Hui, C.K.M.; Hull, J.H.; Birring, S.S.; McGarvey, L.; Mazzone, S.B.; Chung, K.F. Confronting COVID-19-associated cough and the post-COVID syndrome: Role of viral neurotropism, neuroinflammation, and neuroimmune responses. *Lancet Resp. Med.* **2021**, *9*, 533–544. [[CrossRef](#)]
4. Bchetnia, M.; Girard, C.; Duchaine, C.; Laprise, C. The outbreak of the novel severe acute respiratory syndrome coronavirus 2 (SARS-CoV-2): A review of the current global status. *J. Infect. Public Health* **2020**, *13*, 1601–1610. [[CrossRef](#)]
5. Zhu, N.; Zhang, D.; Wang, W.; Li, X.; Yang, B.; Song, J.; Zhao, X.; Huang, B.; Shi, W.; Lu, R.; et al. China Novel Coronavirus, T. Research, A Novel Coronavirus from Patients with Pneumonia in China, 2019. *N. Engl. J. Med.* **2020**, *382*, 727–733. [[CrossRef](#)]
6. Leung, W.W.F.; Sun, Q. Electrostatic charged nanofiber filter for filtering airborne novel coronavirus (COVID-19) and nano-aerosols. *Sep. Purif. Technol.* **2020**, *250*, 116886. [[CrossRef](#)]
7. Asselah, T.; Durantel, D.; Pasmant, E.; Lau, G.; Schinazi, R.F. COVID-19: Discovery, diagnostics and drug development. *J. Hepatol.* **2021**, *74*, 168–184. [[CrossRef](#)]
8. Menni, C.; Valdes, A.M.; Polidori, L.; Antonelli, M.; Penamakuri, S.; Nogal, A.; Louca, P.; May, A.; Figueiredo, J.C.; Hu, C.; et al. Symptom prevalence, duration, and risk of hospital admission in individuals infected with SARS-CoV-2 during periods of omicron and delta variant dominance: A prospective observational study from the ZOE COVID Study. *Lancet* **2022**, *399*, 1618–1624. [[CrossRef](#)]
9. Yim, J.; Lim, H.H.; Kwon, Y. COVID-19 and pulmonary fibrosis: Therapeutics in clinical trials, repurposing, and potential development. *Arch. Pharm. Res.* **2021**, *44*, 499–513. [[CrossRef](#)]
10. Pavli, A.; Theodoridou, M.; Maltezou, H.C. Post-COVID Syndrome: Incidence, Clinical Spectrum, and Challenges for Primary Healthcare Professionals. *Arch. Med. Res.* **2021**, *52*, 575–581. [[CrossRef](#)]
11. Huang, J.; Tao, G.; Liu, J.; Cai, J.; Huang, Z.; Chen, J.-x. Current Prevention of COVID-19: Natural Products and Herbal Medicine. *Front. Pharmacol.* **2020**, *11*, 588508. [[CrossRef](#)] [[PubMed](#)]
12. Fan, A.Y.; Gu, S.; Alemi, S.F. Research Group for Evidence-based Chinese, Chinese herbal medicine for COVID-19: Current evidence with systematic review and meta-analysis. *J. Integr. Med.* **2020**, *18*, 385–394. [[CrossRef](#)] [[PubMed](#)]
13. Tejera, E.; Pérez-Castillo, Y.; Toscano, G.; Noboa, A.L.; Ochoa-Herrera, V.; Giampieri, F.; Álvarez-Suarez, J.M. Computational modeling predicts potential effects of the herbal infusion “horchata” against COVID-19. *Food Chem.* **2022**, *366*, 130589. [[CrossRef](#)]
14. Wang, S.; Zeng, X.; Wang, Y.; Zhao, Y.; Chen, W.; Chen, Y.Z. East meets West in COVID-19 therapeutics. *Pharmacol Res.* **2020**, *159*, 105008. [[CrossRef](#)]
15. Shin, N.R.; Ryu, H.W.; Ko, J.W.; Park, S.H.; Yuk, H.J.; Kim, H.J.; Kim, J.C.; Jeong, S.H.; Shin, I.S. Artemisia argyi attenuates airway inflammation in ovalbumin-induced asthmatic animals. *J. Ethnopharmacol.* **2017**, *209*, 108–115. [[CrossRef](#)] [[PubMed](#)]
16. Zhan, J.; He, F.; Chen, S.; Poudel, A.J.; Yang, Y.; Xiao, L.; Xiang, F.; Li, S. Preparation and Antibacterial Activity of Thermo-Responsive Nanohydrogels from Qiai Essential Oil and Pluronic F108. *Molecules* **2021**, *26*, 5771. [[CrossRef](#)] [[PubMed](#)]
17. Song, W.Y.; Ji, H.Y.; Baek, N.-I.; Jeong, T.-S.; Lee, H.S. In Vitro metabolism of Jaceosidin and characterization of cytochrome P450 and UDP-glucuronosyltransferase enzymes in human liver microsomes. *Arch. Med. Res.* **2010**, *33*, 1985–1996. [[CrossRef](#)]
18. Alzaabi, M.M.; Hamdy, R.; Ashmawy, N.S.; Hamoda, A.M.; Alkhatay, F.; Khademi, N.N.; Al Joud, S.M.A.; El-Keblawy, A.A.; Soliman, S.S.M. Flavonoids are promising safe therapy against COVID-19. *Phytochem. Rev.* **2021**, *21*, 291–312. [[CrossRef](#)]

19. Firoz, A.; Talwar, P. COVID-19 and retina COVID-19 and retinal degenerative diseases: Promising link “Kaempferol”. *Curr. Opin. Pharmacol.* **2022**, *64*, 102231. [[CrossRef](#)]
20. Owis, A.I.; El-Hawary, M.S.; Amir, D.E.; Aly, O.M.; Abdelmohsen, U.R.; Kamel, M.S. Molecular docking reveals the potential of *Salvadora persica* flavonoids to inhibit COVID-19 virus main protease. *RSC Adv.* **2020**, *10*, 19570–19575. [[CrossRef](#)]
21. Zrieq, R.; Ahmad, I.; Snoussi, M.; Noumi, E.; Iriti, M.; Algahtani, F.D.; Patel, H.; Saeed, M.; Tasleem, M.; Sulaiman, S.; et al. Tomatidine and Patchouli Alcohol as Inhibitors of SARS-CoV-2 Enzymes (3CLpro, PLpro and NSP15) by Molecular Docking and Molecular Dynamics Simulations. *Int. J. Mol. Sci.* **2021**, *22*, 10693. [[CrossRef](#)] [[PubMed](#)]
22. Hagar, M.; Ahmed, H.A.; Aljohani, G.; Alhaddad, O.A. Investigation of Some Antiviral N-Heterocycles as COVID 19 Drug: Molecular Docking and DFT Calculations. *Int. J. Mol. Sci.* **2020**, *21*, 3922. [[CrossRef](#)] [[PubMed](#)]
23. Kong, R.; Yang, G.; Xue, R.; Liu, M.; Wang, F.; Hu, J.; Guo, X.; Chang, S.; Ponty, Y. COVID-19 Docking Server: A meta server for docking small molecules, peptides and antibodies against potential targets of COVID-19. *Bioinformatics* **2020**, *36*, 5109–5111. [[CrossRef](#)]
24. Hussein, R.K.; Elkhair, H.M. Molecular docking identification for the efficacy of some zinc complexes with chloroquine and hydroxychloroquine against main protease of COVID-19. *J. Mol. Struct.* **2021**, *1231*, 129979. [[CrossRef](#)]
25. Gholivand, K.; Mohammadpanah, F.; Pooyan, M.; Roohzadeh, R. Evaluating anti-coronavirus activity of some phosphoramides and their influencing inhibitory factors using molecular docking, DFT, QSAR, and NCI-RDG studies. *J. Mol. Struct.* **2022**, *1248*, 131481. [[CrossRef](#)] [[PubMed](#)]
26. Ghazwani, M.Y.; Bakheit, A.H.; Hakami, A.R.; Alkahtani, H.M.; Almehezia, A.A. Virtual Screening and Molecular Docking Studies for Discovery of Potential RNA-Dependent RNA Polymerase Inhibitors. *Crystals* **2021**, *22*, 471. [[CrossRef](#)]
27. Kadela-Tomanek, M.; Jastrzębska, M.; Marciniak, K.; Bębenek, E.; Chrobak, E.; Boryczka, S. Spectroscopic Investigations, Computational Analysis and Molecular Docking to SAR-Cov-2 Targets Studies of 5,8-Quinolinedione Attached to Betulin Derivatives. *Crystals* **2021**, *11*, 76. [[CrossRef](#)]
28. Cortes, E.; Mora, J.; Márquez, E. Modelling the Anti-Methicillin-Resistant *Staphylococcus Aureus* (MRSA) Activity of Cannabinoids: A QSAR and Docking Study. *Crystals* **2020**, *10*, 692. [[CrossRef](#)]
29. Motiur Rahman, A.F.M.; Lu, Y.; Lee, H.J.; Jo, H.; Yin, W.; Alam, M.S.; Cha, H.; Kadi, A.A.; Kwon, Y.; Jahng, Y. Linear diarylheptanoids as potential anticancer therapeutics: Synthesis, biological evaluation, and structure-activity relationship studies. *Arch. Pharm. Res.* **2018**, *41*, 1131–1148. [[CrossRef](#)]
30. Lu, Y.; Yin, W.; Alam, M.S.; Kadi, A.A.; Jahng, Y.; Kwon, Y.; Rahman, A.F.M. Synthesis, Biological Evaluation and Molecular Docking Study of Cyclic Diarylheptanoids as Potential Anticancer Therapeutics. *Anticancer Agents Med. Chem.* **2020**, *20*, 464–475. [[CrossRef](#)]
31. Liu, H.; Ye, F.; Sun, Q.; Liang, H.; Li, C.; Li, S.; Lu, R.; Huang, B.; Tan, W.; Lai, L. *Scutellaria baicalensis* extract and baicalein inhibit replication of SARS-CoV-2 and its 3C-like protease in vitro. *J. Enzyme Inhib. Med. Chem.* **2021**, *36*, 497–503. [[CrossRef](#)] [[PubMed](#)]
32. Song, J.; Zhang, L.; Xu, Y.; Yang, D.; Zhang, L.; Yang, S.; Zhang, W.; Wang, J.; Tian, S.; Yang, S.; et al. The comprehensive study on the therapeutic effects of baicalein for the treatment of COVID-19 in vivo and in vitro. *Biochem. Pharmacol.* **2021**, *183*, 114302. [[CrossRef](#)] [[PubMed](#)]
33. Kumari, S.; Carmona, A.V.; Tiwari, A.K.; Trippier, P.C. Amide Bond Bioisosteres: Strategies, Synthesis, and Successes. *J. Med. Chem.* **2020**, *63*, 12290–12358. [[CrossRef](#)] [[PubMed](#)]
34. Rupa, S.A.; Moni, M.R.; Patwary, M.A.M.; Mahmud, M.M.; Haque, M.A.; Uddin, J.; Abedin, S.M.T. Synthesis of Novel Tritopic Hydrazone Ligands: Spectroscopy, Biological Activity, DFT, and Molecular Docking Studies. *Molecules* **2022**, *27*, 1656. [[CrossRef](#)]
35. Yao, C.; Xiang, F.; Xu, Z. Metal oxide nanocage as drug delivery systems for Favipiravir, as an effective drug for the treatment of COVID-19: A computational study. *J. Mol. Model.* **2022**, *28*, 64. [[CrossRef](#)] [[PubMed](#)]
36. Parthiban, A.; Sachithanandam, V.; Lalitha, P.; Elumalai, D.; Asha, R.N.; Jeyakumar, T.C.; Muthukumar, J.; Jain, M.; Jayabal, K.; Mageswaran, T.; et al. Isolation and biological evaluation 7-hydroxy flavone from *Avicennia officinalis* L.: Insights from extensive in vitro, DFT, molecular docking and molecular dynamics simulation studies. *J. Biomol. Struct. Dyn.* **2022**, *2022*, 1–13. [[CrossRef](#)]
37. Xavier, S.; Periandy, S.; Ramalingam, S. NBO, conformational, NLO, HOMO-LUMO, NMR and electronic spectral study on 1-phenyl-1-propanol by quantum computational methods. *Spectrochim Acta A Mol. Biomol. Spectrosc.* **2015**, *137*, 306–320. [[CrossRef](#)]
38. Rathi, P.C.; Ludlow, R.F.; Verdonk, M.L. Practical High-Quality Electrostatic Potential Surfaces for Drug Discovery Using a Graph-Convolutional Deep Neural Network. *J. Med. Chem.* **2020**, *63*, 8778–8790. [[CrossRef](#)]
39. Nittinger, E.; Inhester, T.; Bietz, S.; Meyder, A.K.; Schomburg, T.; Lange, G.; Klein, R.; Rarey, M. Large-Scale Analysis of Hydrogen Bond Interaction Patterns in Protein-Ligand Interfaces. *J. Med. Chem.* **2017**, *60*, 4245–4257. [[CrossRef](#)]